Desalination 522 (2022) 115436

Contents lists available at ScienceDirect

Desalination

journal homepage: www.elsevier.com/locate/desal

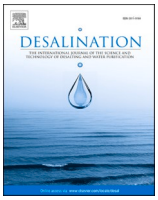

Nanodiamond-decorated thin film composite membranes with antifouling and antibacterial properties

Pooria Karami [a,b,1], Sadegh Aghapour Aktij [a,b,1], Behnam Khorshidi [c], Mostafa Dadashi Firouzjaei [d], Asad Asad [b], Mark Elliott [d], Ahmad Rahimpour [e], João B. P. Soares [a,*], Mohtada Sadrzadeh [b,*]

[a] Department of Chemical & Materials Engineering, 12-263 Donadeo Innovation Centre for Engineering, Group of Applied Macromolecular Engineering, University of Alberta, Edmonton, AB T6G 1H9, Canada
[b] Department of Mechanical Engineering, 10-367 Donadeo Innovation Center for Engineering, Advanced Water Research Lab (AWRL), University of Alberta, Edmonton, AB T6G 1H9, Canada
[c] Department of Chemical Engineering and Applied Chemistry, University of Toronto, Toronto, ON M5S 3E5, Canada
[d] Department of Civil, Construction and Environmental Engineering, University of Alabama, Tuscaloosa 35487, USA
[e] Faculty of Chemical Engineering, Babol Noshirvani University of Technology, Shariati Ave., Babol 47148-71167, Iran

HIGHLIGHTS

- Surface of thin film composite (TFC) membranes was modified using nanodiamond (ND).
- Amine-terminated NDs were covalently attached to surface to form stable membranes.
- The presence of NDs reduced the content of carboxylic groups of polyamide layer.
- ND-modified membranes were antifouling against sodium alginate and protein foulants.
- Amine-functionalized ND inactivated significant ratio of *E-coli* on membrane surface.

ARTICLE INFO

Keywords:
Nanodiamond
Thin film composite membrane
Polyamide
Antifouling properties

ABSTRACT

Membrane fouling is the main bottleneck that restricts the practical applications of membrane processes. In this work, we report an effective and scalable method to reduce the fouling of polyamide thin film composite (TFC) membranes by grafting amine-functionalized nanodiamond (ND) particles. The surface chemistry of ND was modified to improve the compatibility of nanoparticles with the polyamide membranes. Fouling experiments with sodium alginate (SA) and bovine serum albumin (BSA) showed that the ND layer substantially reduced fouling of the membranes. The flux of the ND-modified membrane made with a solution containing 1000 ppm ND particles declined only by 15% (SA) and 9% (BSA) after 180 min of filtration, while the flux of the pristine TFC membrane declined by 42% (SA) and 21% (BSA). The ND particles increased the antibacterial activity of the membranes, increasing the inactivation and mortality rate of *Escherichia coli* (*E. coli*) bacteria cells. Because they are easy to make and have antifouling and antibacterial properties, these membranes can be applied in a broad range of forward osmosis water reclamation applications.

1. Introduction

Significant changes in water consumption patterns, population growth, climate, and urbanization have exacerbated the environmental stresses on available freshwater resources [1,2]. In 2020, the United Nations World Water Development Report (UN WWDR) stated that global water consumption is increasing at a rate of 1% per year, forecasting a 20 to 30% rise by 2050 compared to the current level of water usage [3]. The global need for a safe and clean water supply has urged many countries to explore more efficient water treatment, recycle, and

* Corresponding authors.
E-mail addresses: jsoares@ualberta.ca (J.B.P. Soares), sadrzade@ualberta.ca (M. Sadrzadeh).
[1] Equal contribution.

https://doi.org/10.1016/j.desal.2021.115436
Received 18 August 2021; Received in revised form 27 October 2021; Accepted 28 October 2021
Available online 9 November 2021

reuse solutions. Among water treatment processes, membrane technology has come under the spotlight as a single-step energy-efficient method to desalinate and treat wastewater. Membrane technology offers several attractive features such as portability, high-quality end-product, environmental friendliness, and low operating expenses [4–6].

Osmotically driven membrane processes rely on osmotic pressure differences across a membrane for water recovery. In the forward osmosis (FO) process, the water is drawn from a dilute feed solution with lower osmotic pressure to a concentrated draw solution with higher osmotic pressure [7,8]. Polyamide thin-film composite (TFC) membranes are the most popular FO membranes due to high water fluxes, low salt passages, and high mechanical stabilities. The high permeability of TFC membranes is attributed to their thin (50–200 nm) polyamide selective layer, which is formed on a microporous substrate [9]. One of the main obstacles to the use of FO TFC membranes in wastewater treatment is fouling caused by the deposition/attachment of colloidal particles, organic matter, and solute macromolecules onto the membrane surface. Fouling reduces the performance and lifetime of forward osmosis TFC membranes, hindering their widespread applications for wastewater reclamation [10–12].

Most surface modification methods employed to reduce the fouling of polyamide membranes rely on physical coating or chemical grafting of functional materials on the membrane surface to change its hydrophilicity, surface charge, and roughness [13–17]. The physical coating method, while being versatile, inexpensive, and adaptable to many substrates, suffers from the weak attachment of coatings to the membrane surface and from leaching during cross-flow filtration. The need to make more durable coatings has drawn attention to chemical grafting methods. In this method, hydrophilic macromolecules are either *grafted to* or *grafted from* the membrane surface. The first method refers to tethering hydrophilic polymers to the membrane surface, while the latter to growing polymer chains from the surface. In either method, the need for post-treatment steps, such as plasma or UV treatment, to ensure grafting, as well as the potential danger of releasing grafted materials to the environment, raises concerns about the cost, scalability, and environmental friendliness of these approaches.

Recently, multiple investigations reported an efficient technique to modify the surface of the polyamide layer without post-fabrication treatments [18–21]. In the *chemically induced grafting*, the unreacted dangling acyl chloride (COCl) functional groups that remain from the polyamide polymerization step are modified via nucleophilic substitution reaction with amine-terminated modifiers. Lu et al. [18] modified the polyamide surface with an amine-terminated polyethylene glycol derivative (Jeffamine) to make TFC membranes harder to foul with organic compounds. The Jeffamine-modified membranes had a significantly lower flux decline than the pristine membrane in filtering an alginate solution. The antifouling properties were ascribed to low membrane/foulant interactions, and to higher hydrophilicity of amine-modified TFC membranes.

Inorganic nanoparticles are usually unsuitable for coating polyamide because they are incompatible with the membrane surface and tend to agglomerate during the coating process [22]. Yin et al. [19] coated the surface of a polyamide TFC membrane with silver nanoparticles by first reacting the polyamide layer with NH_2-$(CH_2)_2$-SH (cysteamine), then by attaching antibacterial silver nanoparticles over the polyamide layer by Ag—S chemical bonding. The affinity of surface chemistry between the nanoparticles and the membrane is a critical prerequisite to translate the properties of inorganic nanoparticles to the antifouling properties of polymeric membranes.

This study aims to graft amine-functionalized nanodiamond (ND) particles to the untreated surface of polyamide membranes to enhance the antifouling and antibacterial properties. ND nanoparticle has a crystalline diamond structure and a heterogeneous graphitic shell. The surface characteristics of the ND particles in terms of available functional groups, such as carbonyls, carboxyls, phenols, pyrones, and sulfonic acids, determine their colloidal properties, surface charge, and intermolecular interactions with the host medium. The presence of oxygen-containing functional groups makes ND particles more hydrophilic. Moreover, the graphitic shell of ND particles, with sp^2 hybridization of carbon atoms, provides tunable surface chemistry for further functionalization [23–27]. In addition, their low toxicity, high chemical stability, and antibacterial properties make ND particles interesting for a broad range of applications [28–31]. Nanodiamond is also a non-cytotoxic antibacterial agent that interferes with biofilm formation [32]. Etemadi et al. [33] showed that amine-functionalized ND and polyethylene glycol-functionalized ND increased the antibacterial and biofilm-disrupting activity of cellulose acetate membranes by reducing the filamentous bacteria/membrane adhesion. Recently, our group developed high-performance thin film nanocomposite membranes through incorporating ND particles *within* the selective layer [30]. The ND particles showed excellent compatibility with the polymeric matrix during the polymerization. ND particles increased water permeability during filtration with a stable separation performance.

In this paper, we showed how TFC membranes could be made more resistant to fouling by grafting ND particles onto the polyamide selective layer. We also proposed a facile method to fabricate ND-modified TFC membranes. The ND particles were first functionalized with ethylenediamine (EDA) to provide adequate surface chemistry for membrane functionalization. Then, the amine-functionalized ND particles were grafted to freshly synthesized polyamide TFC membranes by reacting them with the unreacted acyl chloride functional groups on their surfaces. The membranes' fouling resistance was assessed with a series of forward osmosis filtrations. The enhanced fouling tolerance of the ND-coated TFCs was explained based on the surface chemical composition, wettability, and surface roughness.

2. Experimental methodology

2.1. Chemicals and reagents

Commercial polyethersulfone substrates (200 nm pore size) were purchased from Sterlitech Co. Nanodiamond (3–10 nm particle size) was received from US Research Nanomaterials. *M*-phenylene diamine (MPD, >99%) and trimesoyl chloride (TMC, 98%) were purchased from Sigma-Aldrich. Ethylenediamine (EDA), anhydrous tetrahydrofuran (THF) (≥ 99.9%), and thionyl chloride (≥ 99%) were bought from Sigma-Aldrich. Ethanol, n-heptane, sodium dodecyl sulfate (SDS), and triethylamine (TEA) were acquired from Fisher Scientific. Sodium chloride (NaCl, > 99%) was purchased from Fisher. Sodium alginate (SA, 12–80 kDa, St. Louis, MO) and bovine serum albumin (BSA) were obtained from Sigma-Aldrich and ChemCruz, respectively, and used as the organic foulants. Calcium chloride ($CaCl_2$) was obtained from Fisher Scientific to be added to the foulant solution as a chain cross-linker.

2.2. Preparation of ND-coated membranes

Surface functionalization of ND was carried out with EDA through carboxylation, chlorination, and amination. The carboxylic groups of the ND particles were converted to EDA-terminated functionalities through a wet chemical process (Fig. 1). The details of the functionalizing procedure were presented in our previous publication [34]. An ultra-thin selective layer was fabricated over the porous polyethersulfone support with a step-growth polymerization between MPD and TMC at the interface of DI water and n-heptane [35]. First, the polyethersulfone substrate was soaked with the aqueous MPD solution containing 2 wt% MPD, 1 wt% TEA, and 0.2 wt% SDS for 9 min. After removing the excess amine solution from the polyethersulfone surface using a roller, a 0.4 wt% TMC solution was poured on the substrate for 30 s reaction. The TFC membranes were then functionalized with amine-functionalized ND particles.

Initially, a desired concentration of the ND-EDA powder (250, 500, and 1000 ppm) was loaded in 15 ml of ethanol, followed by sonication in

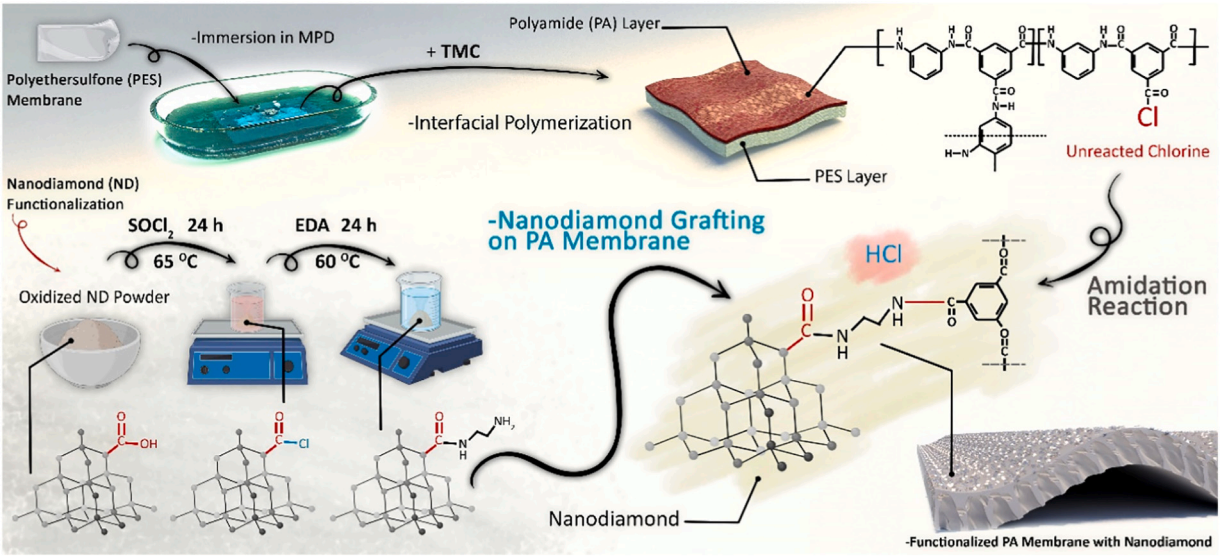

Fig. 1. Schematic representation of interfacial polymerization, ND particle functionalization, and ND particle grafting over the polyamide surface. The ND particles were modified with EDA in order to provide a reactive surface with polyamide COCl groups. The surface of polyamide membrane was coated with ND particles through formation of amide linkages between ND-EDA particles and unreacted COCl groups.

a water bath for 10 min. After that, the ND-EDA dispersion was poured over the polyamide layer to allow the free amine groups of the ND-EDA particles to react with the acyl chloride groups of the polyamide surface. After 10 min, the membranes were rinsed two times with pure ethanol to remove the unreacted ND-EDA particles, and cured in an oven (Thermo Scientific Heratherm™, USA) at 60 °C for 4 min. The membranes were stored in distilled water at room temperature.

The ND-modified membranes prepared with 250 ppm, 500 ppm, and 1000 ppm of ND-EDA were labeled TFC-250, TFC-500, and TFC-1000, respectively. To evaluate the effect of ethanol and functionalized ND particles, a pristine TFC membrane (TFC-0) and a control ethanol-modified TFC membrane (TFC-EtOH) were also fabricated. The TFC-EtOH membrane was made with a pure ethanol solution, following the same procedure used to make the ND surface-modified membranes. The chemical grafting of the TFC membranes with ND-EDA is illustrated in Fig. 1. Detailed information on the physiochemical characterization, experimental details of forward osmosis filtration and fouling experiments, and antibacterial testing methodologies of the fabricated membranes are given in the *Supporting Information*.

3. Results and discussion

3.1. FTIR and TEM analysis of nanodiamond particles

Fig. 2(a) shows the FTIR spectra of the ND, carboxylated ND, and EDA-modified ND (ND-EDA). ND-EDA particles show two peaks at 1530 cm^{-1} (C—N stretching and in-plane bending vibrations of the N—H bond in the amine groups) and 1670 cm^{-1} (C═O stretching vibration of the amide groups), indicating the presence of EDA modifier. The peak at 1670 cm^{-1} is shifted to the right due to the presence of electronegative nitrogen atoms [34,36]. The peak at 1740 cm^{-1} in ND-EDA and carboxylated ND particles is attributed to the free acid band of the

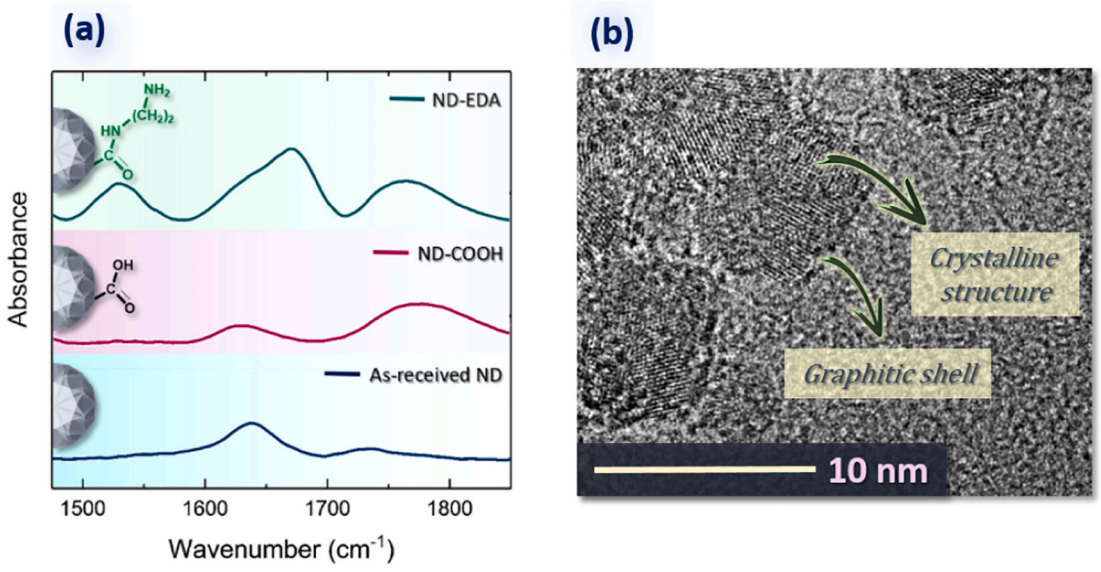

Fig. 2. (a) FTIR spectra of pristine ND, carboxylated ND, and ND-EDA particles and (b) TEM image of nanoparticles. The spherical shape of ND particles represents both diamond core and graphitic shell structures.

carboxylic groups [37]. The TEM image of the ND particles in Fig. 2(b) shows that they are spherical with diameters lower than 10 nm. The crystalline diamond core and the graphitic shell can be distinguished in the TEM image.

3.2. FTIR and XPS results of fabricated TFC membranes

Fig. 3(a) compares the FTIR spectra of the polyethersulfone, TFC-0, TFC-EtOH, and ND-modified TFC membranes. The polyamide peaks at 1660 cm^{-1} (C═O stretching of amide I), 1610 cm^{-1} (aromatic amide ring stretching), and 1540 cm^{-1} (C – N stretching/N-H in-plane bending of amide II) in TFC membranes confirms the formation of polyamide over the polyethersulfone substrate [9,38–41]. The intensity of the polyamide peaks increases as the concentration of the nanoparticles increase, which is related to the formation of amide linkages between amine-terminated ND particles and the COCl groups in the polyamide layer. Fig. 3(b) is a schematic depicting the polyamide membranes before and after ND functionalization.

Fig. 3(c) shows the XPS carbon (C 1s) and nitrogen (N 1s) spectra of the membranes. The functional group ratio of the deconvoluted C 1s and N 1s peaks is summarized in Table 1. The C 1s peak comprises peaks of C-H/C-C at 285 eV, C-COOH/C-CONH at 285.7 eV, CN- at 286.2 eV, N-C═O at 288.4 eV, and O-C═O at 288.5 eV. The N 1s peak comprises peaks of R-NH_2 at 398.5 eV, N-C═O at 400.5 eV, and –$NH3^+$ at 402.1 eV [30,42,43]. Further explanation for each peak is presented in our previous work [30]. The O-C═O peak area percentage, which correlates with the content of carboxylic groups, decreases as the ND concentration increases because of the reaction between aminated ND particles and unreacted COCl functional groups on the polyamide layer (the ND particles stop the hydrolysis of the COCl group by forming amide linkages). The O-C═O peak for TFC-1000 vanishes completely, indicating that nearly all COCl functional groups were consumed for the highest ND loading. Comparing the R-NH_2 peak in the N 1s species, the TFC-500 and TFC-1000 membranes had a substantially higher peak area percentage than the pristine TFC membrane, likely because of presence of free amine groups of the functionalized ND particles. These FTIR and XPS analyses indicate that the ND particles were covalently bonded to the membrane surface.

3.3. Morphological evaluation of the synthesized membranes

Fig. 4 compares the FESEM and TEM images of the polyethersulfone, TFC-0, TFC-EtOH, and ND-modified membranes. The polyamide layers in the TFC-0 and TFC-EtOH membranes showed nodular features resulting from the heterogeneous MPD diffusion in interfacial polymerization [35,44]. Polyamide was also formed in the larger pores of the substrate. Since the monomer concentrations and polymerization conditions were the same for all membranes, the polyamide surface was similar for the TFC-0 and TFC-EtOH membranes. Attaching the ND particles to the membranes, however, changed their surface morphologies, especially for TFC-1000, which is covered with a layer of ND particles. It seems that the ND particles agglomerated on top of the initially attached ND layer, especially when higher ND loadings were used.

The cross-sectional TEM images reveal that the polyamide thickness in all TFC membranes are similar. The ND-modified TFC membranes,

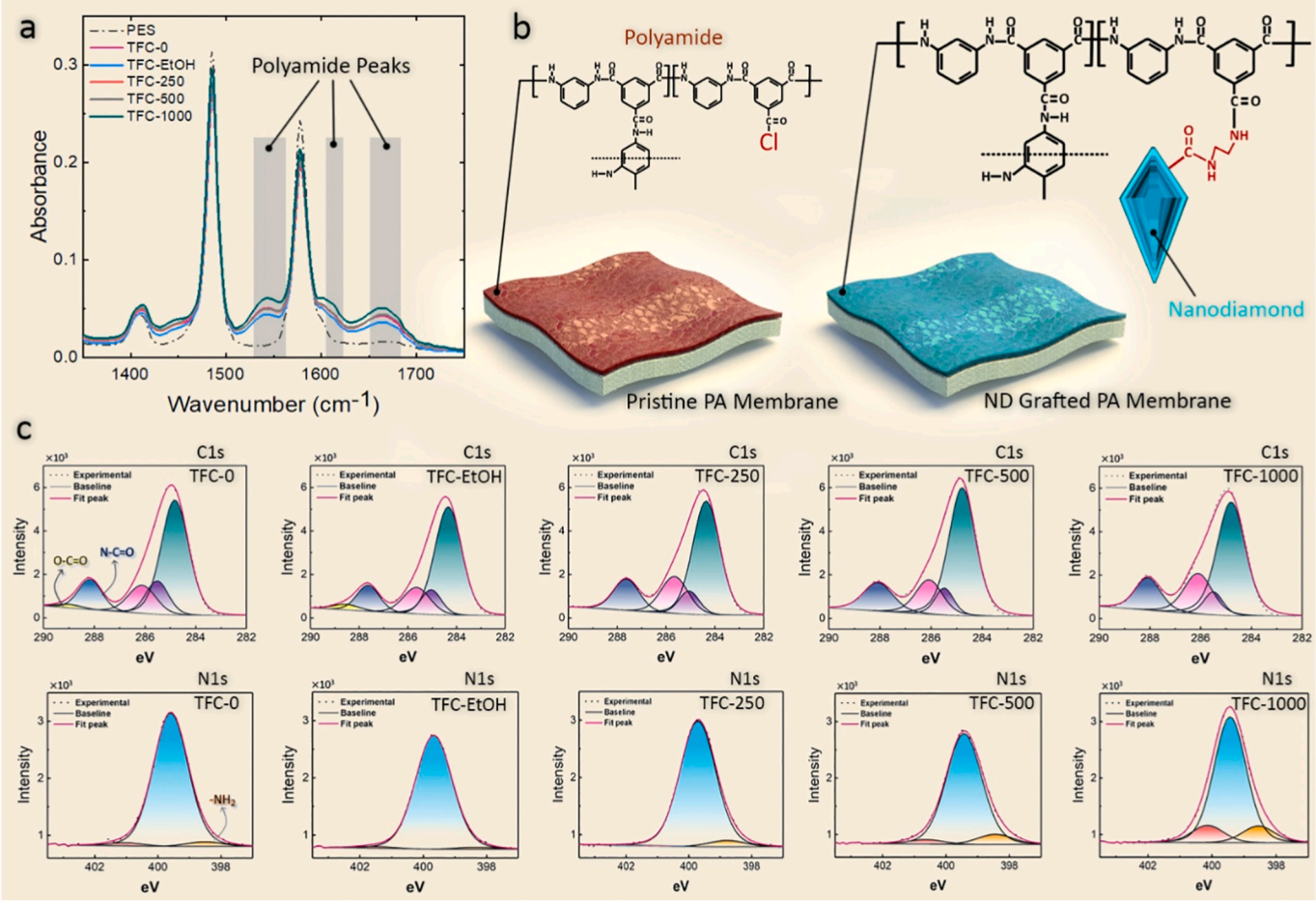

Fig. 3. (a) FTIR spectra of polyethersulfone and fabricated membranes, (b) schematic of TFC membranes before and after ND grafting, and (c) deconvoluted carbon and nitrogen XPS peaks of all synthesized membranes.

Table 1
Peak area percentages of deconvoluted carbon and nitrogen peaks.

Membrane	Functional group ratio (carbon) (%)					Functional group ratio (Nitrogen) (%)		
	C-H/C-C	C-COO/C-CON	CN-	N-C=O	O-C=O	$R\text{-}NH_2$	N-C=O	$\text{-}NH_3^+$
TFC-0	57.43	13.76	14.08	12.94	1.81	2.18	94.53	3.28
TFC-EtOH	59.72	10.35	14.64	12.13	3.16	1.51	96.74	1.74
TFC-250	57.26	8.81	18.67	15.00	0.26	4.81	94.73	0.47
TFC-500	61.17	6.98	17.24	14.39	0.25	8.09	88.28	3.63
TFC-1000	56.98	7.73	20.36	14.96	0.00	10.45	78.96	10.86

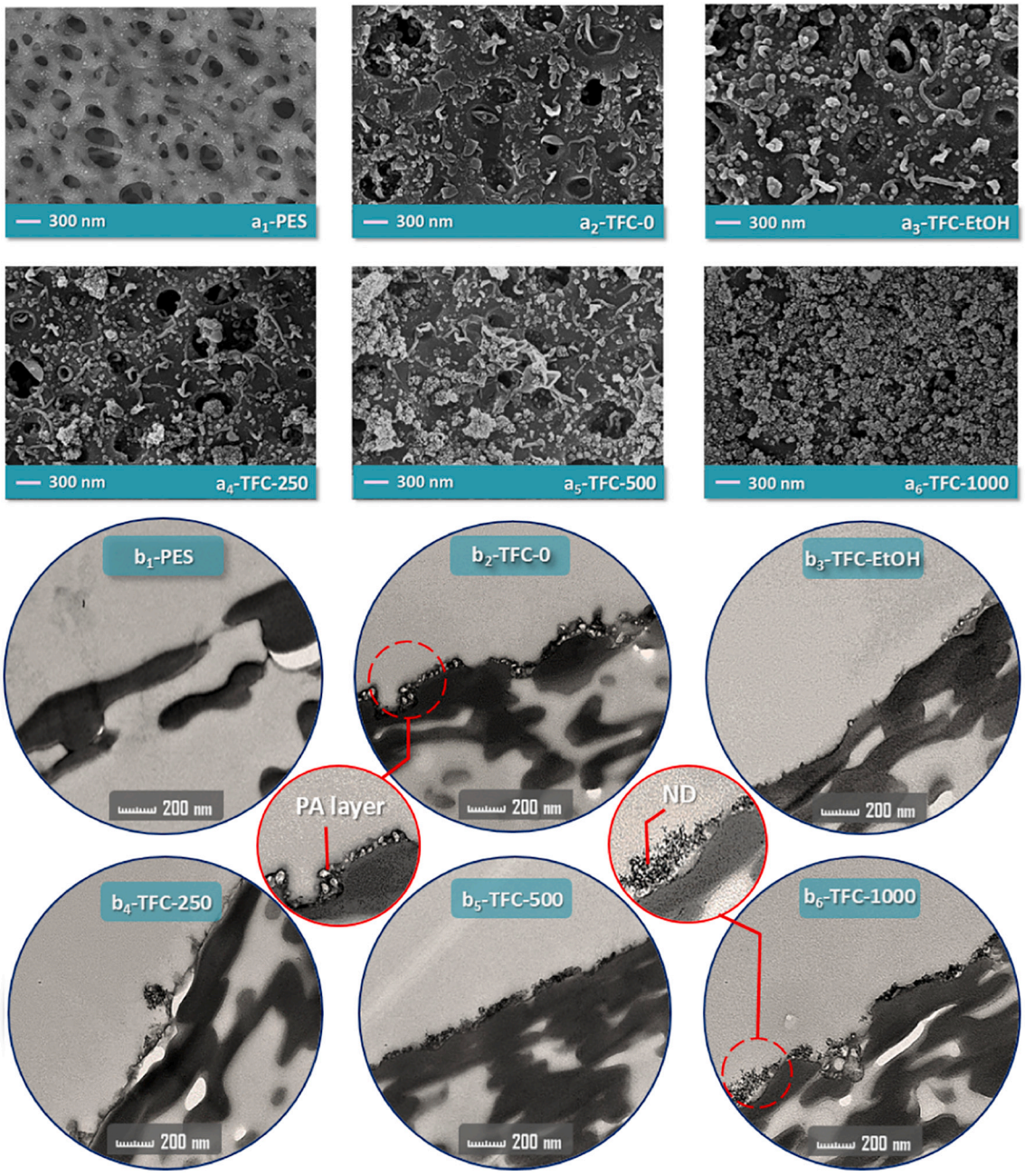

Fig. 4. (a) Top surface FESEM and (b) cross-section TEM images of polyethersulfone, TFC-0, TFC-EtOH, and ND-modified membranes. The membranes modified with ND particles show the presence of nanoparticles on the top surface, which become more distinguishable at higher ND loadings. The polyamide layer in panel b_2-TFC-0 represents the internal void structure which is mostly covered in the TEM images of ND-modified TFC membranes.

especially for higher ND loadings, revealed the nanoparticles over the membrane surface. The TFC-500 and TFC-1000 membranes showed high loading of NDs over the membrane surface, implying the deposition of multiple layers of ND particles on the initially covalently bonded ND particles. TEM images of all TFC membranes showed that the polyamide layer formed continuously on the top surface and inside the pores of the

polyethersulfone support. It indicated that the visible pores on the surface of TFC-0, TFC-EtOH, and TFC-250 were filled with polyamide during the polymerization.

Fig. 5 contrasts the 3D AFM surface topography, surface roughness (R_a and R_q), and water contact angle of the TFCs. The 3D AFM surface topographies show that the membranes have a ridge-and-valley surface structure [45]. The roughness data indicate that the ND layer smoothened the polyamide surface because the nanoparticles filled the "valleys" of the polyamide surface. The water contact angle results show that the surface wettability of the membranes increased when more ND particles were added to the polyamide surface. The water contact angle depends on the surface chemistry and on the morphology of the polyamide layer. Wenzel's model states that for a surface with a contact angle of less than 90° (a wettable surface), a rise in surface roughness should reduce the water contact angle [46]. Our contact angle results, however, disagree with Wenzel's model, since the lowest contact angle was measured for the smoothest membrane (TFC-1000). This observation highlights how the hydrophilicity of the nanoparticles increases the surface wettability of TFC membranes.

3.4. Transport performance of the membranes

Fig. 6(a and b) shows the water flux of the TFC membranes at different draw solution concentrations in two different configurations: active layer facing feed solution (AL-FS) and active layer facing draw solution (AL-DS). In both configurations, the water flux increased with increasing the draw solution concentration. It is due to the buildup of a larger osmotic driving force. However, the water flux increased non-linearly with a lower slope at higher NaCl concentrations, because Na^+ and Cl^- ions accumulated on the polyamide layer in the AL-DS configuration (external concentration polarization, ECP) and within the polyethersulfone layer in the AL-FS configuration (internal concentration polarization, ICP), which reduced the effective osmotic pressure gradient across the membranes [47]. This effect intensified at higher concentrations of the draw solution. Furthermore, the water flux was higher in the AL-DS than in the AL-FS configuration, revealing the more significant effect of ICP in AL-FS compared to ECP in AL-DS on the effective osmotic driving force. The water fluxes through all ethanol-treated membranes (TFC-EtOH and ND-modified TFCs) were higher than in the pristine TFC-0 membrane. The water flux, however, decreased when the loading of ND particles increased. The higher water fluxes of the EtOH-treated membranes are likely a result of the plasticization of the polyamide layer by ethanol [48]. As the polyamide layer swells, the free volume in the polymeric structure increases, making it easier for water to permeate. In addition, ethanol can remove smaller polymer chains that were not bonded to the polyamide network during interfacial polymerization [19]. The reduction of the water flux for ND-coated TFCs, especially at higher loadings, can be related to the additional resistance of the ND layer against water permeation. The size of the covalently attached nanodiamonds and their agglomerates are presumably larger than the size of the water channels in the polyamide selective layer. Therefore, a likely explanation for the flux decline can be the additional transport resistance imposed by the ND layer.

Fig. 6(c and d) compares the reverse salt flux and specific salt flux in both membrane configurations with a 2 M NaCl draw solution. The ethanol-treated TFC membranes (TFC-EtOH and ND-modified TFCs) exhibited higher reverse salt fluxes in both modes than the pristine TFC-0 membrane, which might be related to the swelling effect of alcohol on the selective layer. The TFC-250 and TFC-500 membranes had reverse salt fluxes similar to the TFC-EtOH membrane, showing that ND grafting did not affect salt separation substantially. Higher loadings of ND particles, however, improved salt selectivity: TFC-1000 had the lowest reverse salt flux among all ethanol-treated membranes.

Fig. 6(e) shows the transport parameters (*A, B,* and *S*) of the TFC membranes. The water and solute permeability parameters followed a trend similar to water flux and reverse salt flux in which the ethanol-

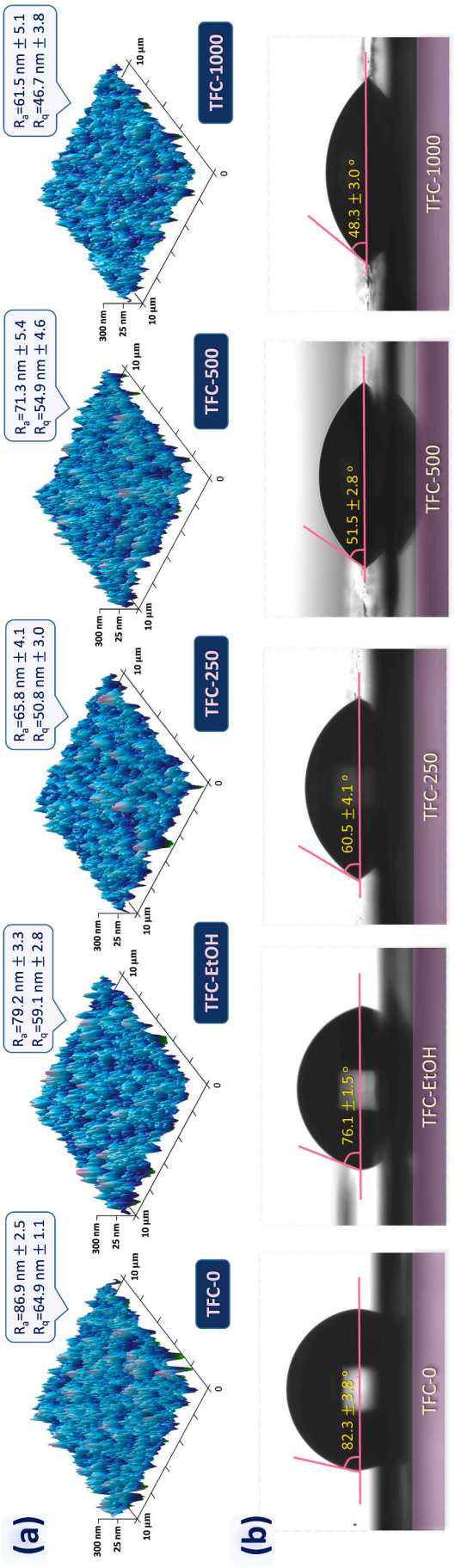

Fig. 5. (a) 3D AFM images, R_a: average roughness, and R_q: root mean square roughness, (b) water contact angle of membranes. All the 3D AFM images are presented with a same z-axis aspect ratio to give a better visual comparison.

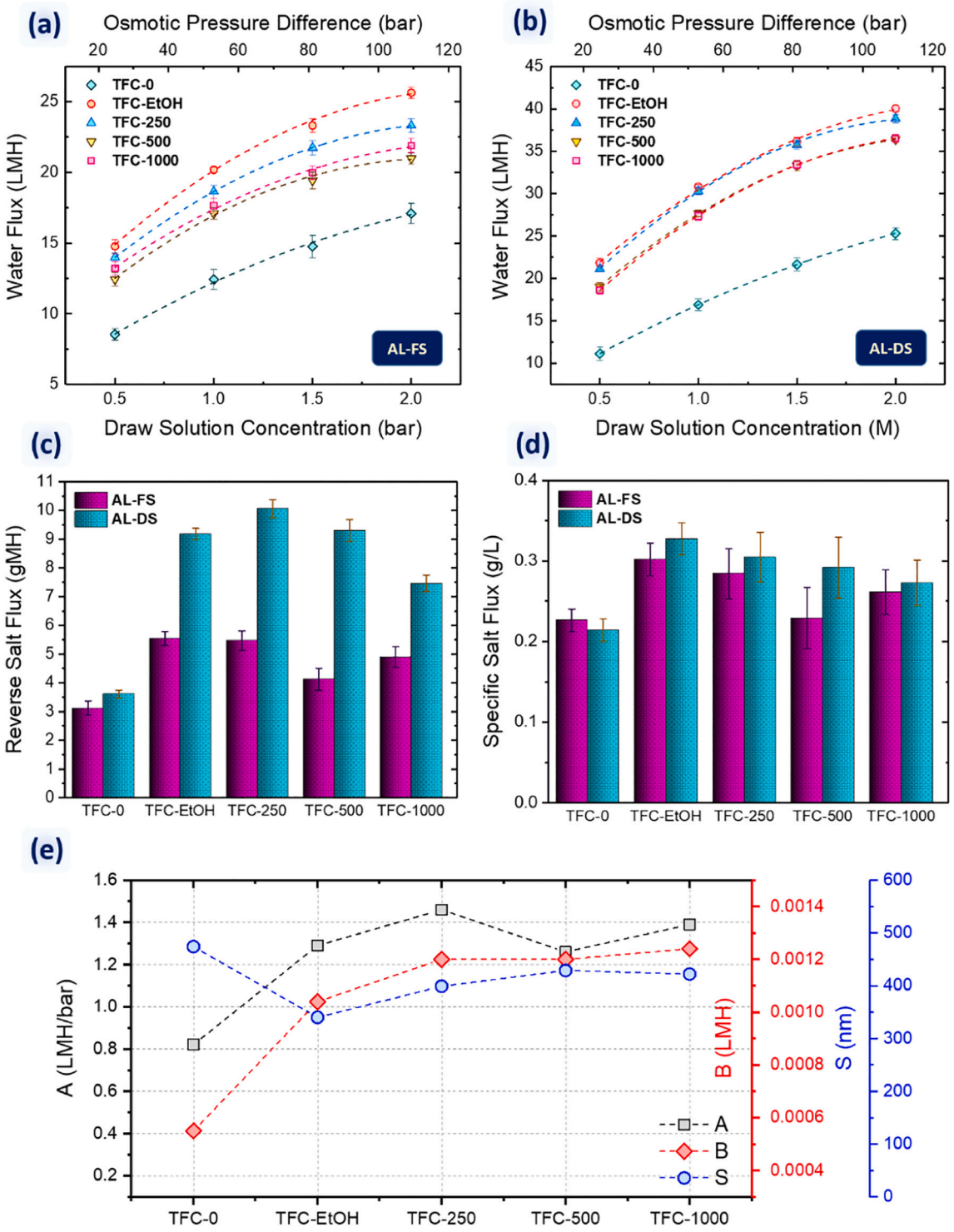

Fig. 6. (a) Water flux in AL-FS configuration, (b) Water flux in AL-DS configuration, (c) reverse salt flux, (d) specific salt flux, and (e) transport parameters for TFC-0, TFC-EtOH, and ND-modified membranes. All the forward osmosis filtrations in AL-FS and AL-DS configurations were performed with 1 M NaCl draw solution and deionized water as the feed solution. The reported water flux in panel a and b is the flux at the beginning of the filtrations. The reverse salt flux is also calculated by measuring the NaCl concentration in feed solution during 2 h filtration.

treated membranes had higher water permeation and lower salt selectivity. The structural parameter, S, is one of the important parameters of polyethersulfone support. The lower structural parameter indicates less severe internal concentration polarization in the support layer of TFC membranes. Since similar polyethersulfone supports were used to fabricate all TFC membranes, the structural parameter showed an average value of 412.8 nm with ±43.8 nm variation.

3.5. *Antifouling properties of ND-modified membranes*

Fig. 7(a and b) shows the water flux during the filtration in the AL-FS configuration for SA-$CaCl_2$ and BSA-$CaCl_2$ feed solutions. The flux of the TFC-0 and TFC-EtOH membranes declined substantially in the initial 30 min of filtration of the SA solution because the organic foulant was accumulated on the membrane. In contrast, the fluxes of the ND-

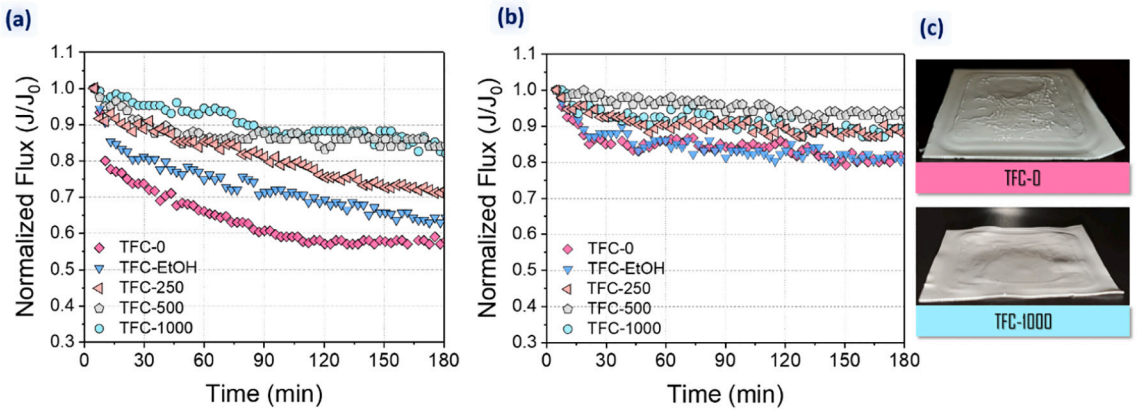

Fig. 7. Water flux of synthesized membranes with (a) SA feed solution and (b) BSA feed solution, (c) formation of alginate gel on TFC-0 and TFC-1000 membranes after 180 min fouling experiment. The abrupt flux decline of TFC-0 in the initial 30 min of the filtration is an indication of alginate cake layer formation. Fouling experiments started with 18±1 LMH water flux for all TFC membranes to exclude the effect of hydrodynamic flow condition on the fouling.

modified membranes declined gradually over the fouling experiments and stabilized after 150 min. Moreover, the flux decline was lower for the TFC membranes with higher ND loadings: TFC-0 had the highest (42%) and TFC-1000 had the least (15%) flux declines of all membranes.

Fig. 7(b) shows that the membranes experienced lower flux declines with the BSA solution, suggesting that the BSA foulant attaches less effectively onto the membrane surfaces. The TFC-0 and TFC-EtOH membranes had similar flux declines in the first 30 min, followed by a gradual decline until the end of the experiments. All the ND-modified membranes were more resistant to BSA fouling, with less than 11% flux decline in 180 min. Fig. 7(c) illustrates that more alginate gel was formed over the membrane surface of the pristine membrane at the end of filtration with SA than with the TFC-1000 membrane.

The fouling mechanism of polyamide membranes can explain why the SA solution caused more fouling than the BSA solution. The presence of Ca^{2+} ions has a major impact on the fouling severity of these membranes because Ca^{2+} ions form cross-linked foulant networks through binding with the carboxylic groups of the foulants. Ca^{2+} ions can also link foulants and carboxylic groups of the polyamide layer (hydrolyzed COCl groups), forming an adhesive fouling layer. These Ca^{2+} attachments are known as Ca^{2+} bridging effect [49,50]. Therefore, the content of carboxylic groups in the foulant and on the polyamide layer can affect the extent of fouling. The BSA molecules have a much lower fraction of carboxylic groups than those of SA. Hence, fewer cross-linked structures form when the feed solution contains BSA and $CaCl_2$, leading to less fouling and lower flux decline. TFC membranes coated with nanoparticles had a lower flux decline, likely because of the fewer carboxylic groups on the ND-modified polyamide layer. As shown by XPS analysis, the amine-functionalized ND particles consumed the COCl groups at the polyamide surface. Therefore, fewer COCl functional groups remained to be hydrolyzed and converted to COOH when rinsing with water. This led to the reduction of adhesion spots on the polyamide layer for Ca^{2+} to make bridges between the membrane and the foulant molecules. The existence of multiple carboxylic groups on the TFC-0 and TFC-EtOH membranes made them more prone to fouling with the foulants. In addition, the hydrophilic ND particles make a hydration layer, and therefore hinder the accumulation of hydrophobic SA and BSA foulants on the surface. Finally, A smoother polyamide film (based on roughness data) is expected to experience less fouling because it has fewer ridges and valleys where foulant molecules can be deposited [51].

3.6. Stability of grafted ND particles

The release rate of ND particles is an indication of the stability and lifetime of the ND layer. Fig. 8 shows the leaching rate of ND particles, measured by the total organic carbon (TOC) over 16 days. On day 1, the

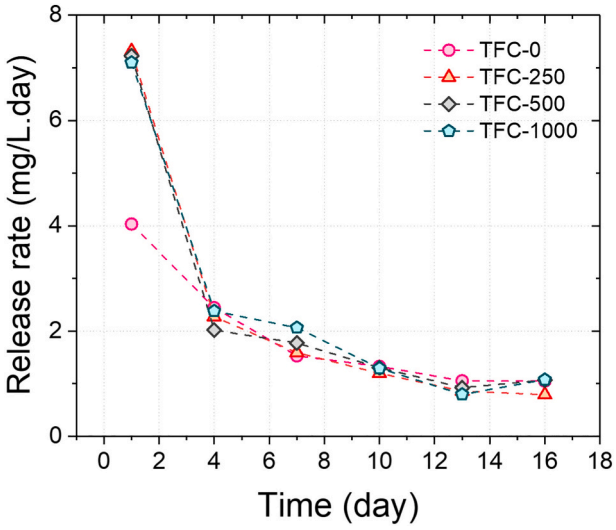

Fig. 8. The release rate of ND particles, evaluated by total organic carbon, for the fabricated membranes. The samples were collected each three days for the analysis. The vials of the samples were refilled with pure water every day to report the release data daily.

release rate of pristine (TFC-0) and ND-modified membranes differed significantly. The release from the pristine membrane is caused by unreacted monomers and residual solvents. The release from the ND-modified TFC membranes is related to the detachment of ND particle agglomerates, unreacted monomers, and residual solvents. It seems that the number of loosly detached ND particles is higher than covalently attached ND partilces as many nanoparticles formed agglomorates over the initially attached layer by weak interactions. However, the leaching curves of all TFC membranes behaved similarly after day 4, suggesting that the ND particles remained on the surface after the loosely attached ND particles were released. The FESEM and TEM analyses showed that the agglomerated ND particles accumulated on top of the covalently-bonded ND layer. The ND agglomerates can be released from the membrane due to their weak interparticle electrostatic interaction, but not the covalently-bonded ND particles.

3.7. Antibacterial activity of the ND membranes

Fig. 9(a) shows a schematic of the colony plating and confocal microscopy tests. The membranes were first exposed to *E. coli* cultures for 3 h, and then monitored through the colony plating (Fig. 9(b_1-b_6)) and

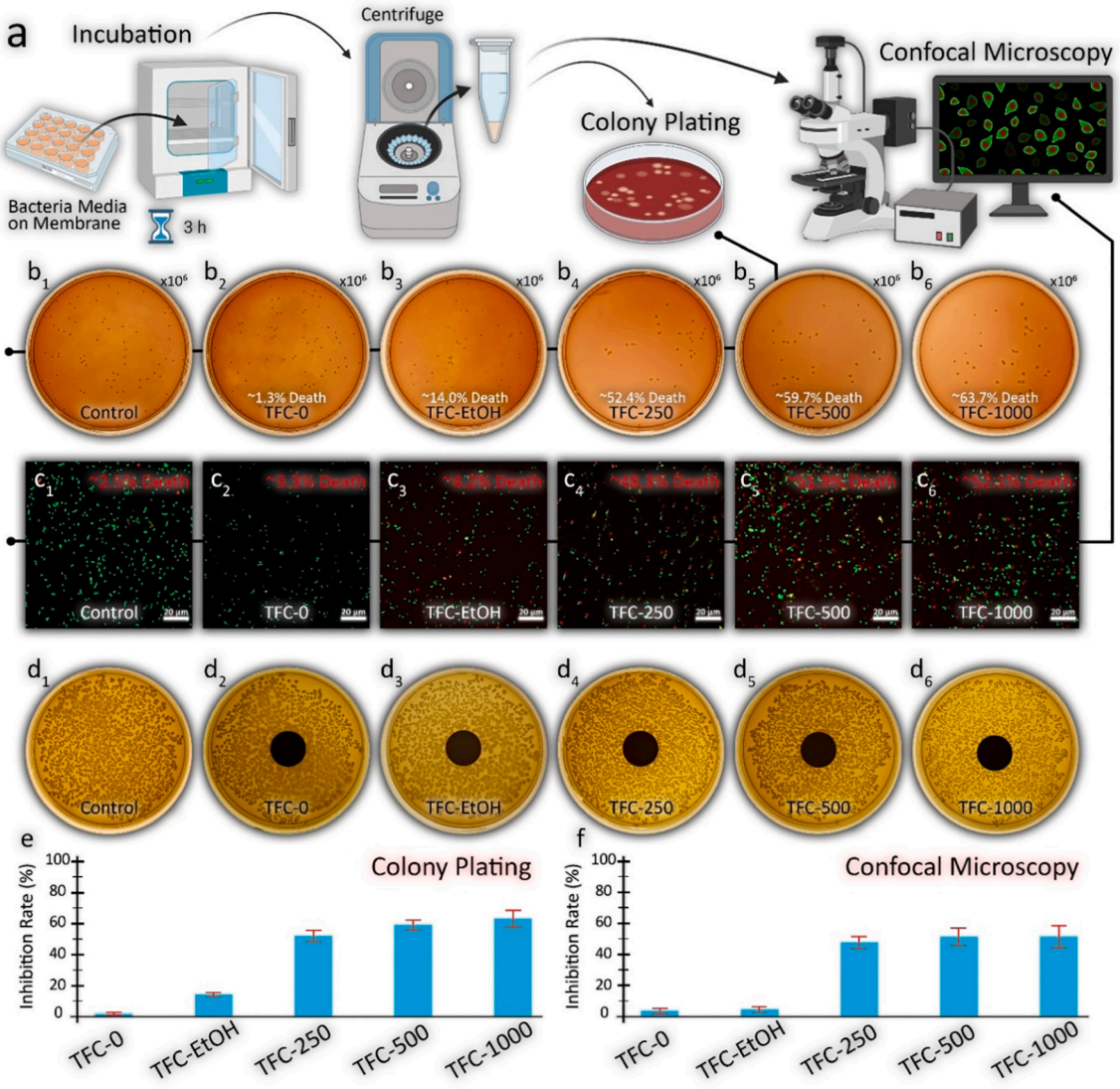

Fig. 9. The antibacterial assessment of the ND membranes. (a) schematic illustration of colony plating and confocal microscopy tests preparation steps, (b1-b6) colony plating test of the membranes. The Solution for these plates has been 10^{-6} diluted. (c1-c6) confocal microscopy test of the membranes (green and red areas represent the live and dead bacteria, respectively). The mortality rate is the ratio of the red area to the total red and green area calculated using ImageJ software, and (d1-d6) inhibition zone test of the membranes (black circles (d2-d6) are the membrane samples). Bacteria inhibition rates of the membranes in (e) colony plating and (f) confocal microscopy tests. (For interpretation of the references to colour in this figure legend, the reader is referred to the web version of this article.)

confocal microscopy (Fig. 9(c_1-c_6)) analyses. *E. coli* was used as one of the common gram-negative bacteria for study of the efficiency of anbacterial agents [52,53]. Control samples were used to calculate the mortality rate of *E. coli* in contact with the membranes. The colony plating test showed that the TFC-1000, TFC-500, and TFC-250 membranes inactivated 63.7%, 59.7%, and 52.4% of the bacteria, respectively, while the TFC-0 and TFC-EtOH membranes inactivated only 1.3% and 14%, respectively. Confocal microscopy results confirmed these findings: The TFC-1000, TFC-500, and TFC-250 membranes showed 52.1%, 51.9%, and 48.3% mortality rates, respectively, while the TFC-0 and TFC-EtOH membranes inhibited a negligible fraction of *E. coli*.

These results confirm that the ND particles significantly increased the bacterial inactivation rates of the membranes. Nanodiamond had already been proven to be a promising antibacterial agent [54,55], and this finding was reflected in the performance of the TFC-1000, TFC-500, and TFC-250 membranes [56]. The colony plating and confocal analysis indicate that higher grafted nanoparticles increase the antibacterial activity of the membranes, but the small difference in inactivation rates between the TFC-1000 and TFC-500 membranes suggests that the membrane surface approaches saturation at this concentration range for inactivating bacteria.

The antibacterial activity of the membranes can be related to the remaining hydroxyl and carbonyl groups on the ND surface (see Fig. 1), since they have been listed as strong antibacterial agents on ND particles by Wehling et al. [54]. These oxygen-containing groups may attach to the intracellular components of the bacteria or bind to their cell walls. This bondage inhibits vital proteins and enzymes, which leads to a rapid collapse of the bacterial metabolism and death [54]. Physical interactions among ND particles and bacteria can be another mechanism for *E. coli* death, as Chatterjee et al. [57] showed in their study. They also mentioned that the interaction of ND with bacteria might be due to the highly reactive surface of ND particles. This increases the chance for a physical hit to the bacterial outer membrane, and eventually causes death.

Disc inhibition zone tests (Fig. 9(d_1-d_6)) demonstrate the antibacterial behavior of the modified TFCs. Inhibition zones form when ions or other antibacterial agents can move away from the membrane by diffusion [58–61]. None of the membranes (black circles in panels d_2-d_6)

showed any inhibition zone surrounding them (in the perimeter of the membranes). This supports the idea that the ND particles are strongly bonded over the polyamide layer. The bondage of nanoparticles to the membrane surface affects the long-term activity of polymeric membranes, especially for anti-biofouling studies. Based on the antibacterial activity of the membranes, it can be concluded that not only functionalization of membranes with ND particles increase the antibacterial activity of the membrane but may also guarantee their long-term performance in the presence of bacteria.

4. Conclusion

A series of ND-modified TFC membranes were synthesized by covalently bonding amine-functionalized ND particles to polyamide layers to explore whether the ND particles formed an antifouling and antibacterial layer. Ethylenediamine was used as the surface modifier to improve the affinity between the functional groups of ND particles and the polyamide. The ND particles reduced fouling of the TFC membranes with SA and BSA organic foulants by decreasing the electrostatic and hydrophobic foulant/membrane interactions, and by reducing the membrane roughness. The ND particles also imparted antibacterial activity to the membranes by killing *E. coli* bacteria cells. Due to their attractive features, such as facile surface modification, reasonable price, hydrophilicity, and the easily implemented grafting methodology proposed in this article, ND-modified TFC membranes are viable alternatives to membranes that contain chemically attached antifouling layers.

CRediT authorship contribution statement

Pooria Karami: Conceptualization, Methodology, Validation, Writing - Original Draft, Investigation, Sadegh Aghapour Aktij: Conceptualization, Methodology, Validation, Writing - Original Draft, Investigation, Behnam Khorshidi: Methodology, Writing- Reviewing and Editing, Investigation, Mostafa Dadashi Firouzjaei: Methodology, Writing-Reviewing and Editing, Investigation, Asad Asad: Methodology, Investigation, Mark Elliott: Methodology, Writing- Reviewing and Editing, Investigation, Ahmad Rahimpour: Methodology, Writing- Reviewing and Editing, Investigation, João B.P. Soares: Supervision, Writing-Reviewing and Editing, Project administration, Funding acquisition, Resources, Mohtada Sadrzadeh: Supervision, Writing- Reviewing and Editing, Project administration, Funding acquisition, Resources.

Declaration of competing interest

The authors declare that they have no known competing financial interests or personal relationships that could have appeared to influence the work reported in this paper.

Acknowledgment

The financial support for this work by the Natural Science and Engineering Research Council of Canada and Canada's Oil Sands Innovation Alliance is gratefully acknowledged. P.K. and S.A.A. acknowledge the financial support (Alberta Innovates Graduate Student Scholarship, AIGSS) from Alberta Innovates of the Alberta government, Canada.

Appendix A. Supplementary data

Supplementary data to this article can be found online at https://doi.org/10.1016/j.desal.2021.115436.

References

[1] P.J.J. Alvarez, C.K. Chan, M. Elimelech, N.J. Halas, D. Villagrán, Emerging opportunities for nanotechnology to enhance water security, Nat. Nanotechnol. 13 (2018) 634.
[2] M.S. Mauter, I. Zucker, F. Perreault, J.R. Werber, J.-H. Kim, M. Elimelech, The role of nanotechnology in tackling global water challenges, Nat. Sustain. 1 (2018) 166–175.
[3] The United Nations World Water Development Report 2020. https://www.unwater.org/publications/world-water-development-report-2020/. (Accessed 2 June 2020).
[4] A.K. Shukla, J. Alam, M. Alhoshan, L.A. Dass, M.R. Muthumareeswaran, Development of a nanocomposite ultrafiltration membrane based on polyphenylsulfone blended with graphene oxide, Sci. Rep. 7 (2017) 1–12.
[5] P. Karami, B. Khorshidi, M. McGregor, J.T. Peichel, J.B.P. Soares, M. Sadrzadeh, Thermally stable thin film composite polymeric membranes for water treatment: a review, J. Clean. Prod. 250 (2020), 119447.
[6] A. Asad, D. Sameoto, M. Sadrzadeh, Overview of membrane technology, in: Nanocomposite Membr. Water Gas Sep, Elsevier, 2020, pp. 1–28.
[7] S. Zhao, L. Zou, C.Y. Tang, D. Mulcahy, Recent developments in forward osmosis: opportunities and challenges 396 (2012) 1–21.
[8] T.-S. Chung, S. Zhang, K.Y. Wang, J. Su, M.M. Ling, Forward osmosis processes: yesterday, today and tomorrow, Desalination 287 (2012) 78–81.
[9] B. Khorshidi, T. Thundat, B.A. Fleck, M. Sadrzadeh, A novel approach toward fabrication of high performance thin film composite polyamide membranes, Sci. Rep. 6 (2016) 22069.
[10] M.D. Firouzjaei, S.F. Seyedpour, S.A. Aktij, M. Giagnorio, N. Bazrafshan, A. Mollahosseini, F. Samadi, S. Ahmadalipour, F.D. Firouzjaei, M.R. Esfahani, Others, recent advances in functionalized polymer membranes for biofouling control and mitigation in forward osmosis, J. Membr. Sci. 596 (2020), 117604.
[11] M.D. Firouzjaei, A.A. Shamsabadi, S.A. Aktij, S.F. Seyedpour, M. Sharifian Gh, A. Rahimpour, M.R. Esfahani, M. Ulbricht, M. Soroush, Exploiting synergetic effects of graphene oxide and a silver-based metal–organic framework to enhance antifouling and anti-biofouling properties of thin-film nanocomposite membranes, ACS Appl.Mater. Interfaces 10 (2018) 42967–42978.
[12] S. Yadav, H. Saleem, I. Ibrar, O. Naji, A.A. Hawari, A.A. Alanezi, S.J. Zaidi, A. Altaee, J. Zhou, Recent developments in forward osmosis membranes using carbon-based nanomaterials, Desalination 482 (2020), 114375.
[13] B. Mi, M. Elimelech, Organic fouling of forward osmosis membranes: fouling reversibility and cleaning without chemical reagents, J. Membr. Sci. 348 (2010) 337–345.
[14] Y. Chun, D. Mulcahy, L. Zou, I.S. Kim, A short review of membrane fouling in forward osmosis processes, Membranes (Basel). 7 (2017) 30.
[15] W.J. Lee, Z.C. Ng, S.K. Hubadillah, P.S. Goh, W.J. Lau, M.H.D. Othman, A.F. Ismail, N. Hilal, Fouling mitigation in forward osmosis and membrane distillation for desalination, Desalination 480 (2020), 114338.
[16] Z. Liu, X. An, C. Dong, S. Zheng, B. Mi, Y. Hu, Modification of thin film composite polyamide membranes with 3D hyperbranched polyglycerol for simultaneous improvement in their filtration performance and antifouling properties, J. Mater. Chem. A 5 (2017) 23190–23197.
[17] M.F. Ismail, M.A. Islam, B. Khorshidi, M. Sadrzadeh, Prediction of surface charge properties on the basis of contact angle titration models, Mater. Chem. Phys. 258 (2021), 123933.
[18] M.E. Xinglin Lu, Santiago Romero-Vargas Castrillón, Devin L. Shaffer, Jun ma, in situ surface chemical modification of thin-film composite forward osmosis membranes for enhanced organic fouling resistance, Environ. Sci. Technol. 47 (2013) 12219–12228.
[19] J. Yin, Y. Yang, Z. Hu, B. Deng, Attachment of silver nanoparticles (AgNPs) onto thin-film composite (TFC) membranes through covalent bonding to reduce membrane biofouling 441 (2013) 73–82.
[20] Q. Guo, J. Li, T. Chen, Q. Yao, J. Xie, Antimicrobial thin-film composite membranes with chemically decorated ultrasmall silver nanoclusters, ACS Sustain. Chem. Eng. 7 (2019) 14848–14855.
[21] S.-H. Park, S.O. Hwang, T.-S. Kim, A. Cho, S.J. Kwon, K.T. Kim, H.-D. Park, J.-H. Lee, Triclosan-immobilized polyamide thin film composite membranes with enhanced biofouling resistance, Appl. Surf. Sci. 443 (2018) 458–466.
[22] G.-R. Xu, J.-N. Wang, C.-J. Li, Strategies for improving the performance of the polyamide thin film composite (PA-TFC) reverse osmosis (RO) membranes: surface modifications and nanoparticles incorporations, Desalination 328 (2013) 83–100.
[23] P. Karami, S. Salkhi Khasraghi, M. Hashemi, S. Rabiei, A. Shojaei, Polymer/nanodiamond composites - a comprehensive review from synthesis and fabrication to properties and applications, Adv. Colloid Interf. Sci. 269 (2019) 122–151.
[24] V.N. Mochalin, Y. Gogotsi, Nanodiamond-polymer composites, Diam. Relat. Mater. 58 (2015) 161–171.
[25] P. Karami, A. Shojaei, Improvement of dry sliding tribological properties of polyamide 6 using diamond nanoparticles, Tribol. Int. 115 (2017) 370–377.
[26] M. Bhadra, S. Roy, S. Mitra, Nanodiamond immobilized membranes for enhanced desalination via membrane distillation, Desalination 341 (2014) 115–119.
[27] M. Raeiszadeh, A. Hakimian, A. Shojaei, H. Molavi, Nanodiamond-filled chitosan as an efficient adsorbent for anionic dye removal from aqueous solutions, J. Environ. Chem. Eng. 6 (2018) 3283–3294.
[28] A. Tizchang, Y. Jafarzadeh, R. Yegani, S. Khakpour, The effects of pristine and silanized nanodiamond on the performance of polysulfone membranes for wastewater treatment by MBR system, J. Environ. Chem. Eng. 7 (2019), 103447.
[29] S. Khakpour, Y. Jafarzadeh, R. Yegani, Incorporation of graphene oxide/nanodiamond nanocomposite into PVC ultrafiltration membranes, Chem. Eng. Res. Des. 152 (2019) 60–70.
[30] P. Karami, B. Khorshidi, L. Shamaei, E. Beaulieu, J.B.P. Soares, M. Sadrzadeh, Nanodiamond-enabled thin-film nanocomposite polyamide membranes for high-temperature water treatment, ACS Appl. Mater. Interfaces 12 (2020) 53274–53285.

[31] V.N. Mochalin, O. Shenderova, D. Ho, Y. Gogotsi, The properties and applications of nanodiamonds, Nat. Nanotechnol. 7 (2012) 11.
[32] V. Turcheniuk, V. Raks, R. Issa, I.R. Cooper, P.J. Cragg, R. Jijie, N. Dumitrascu, L. I. Mikhalovska, A. Barras, V. Zaitsev, Others, antimicrobial activity of menthol modified nanodiamond particles, Diam. Relat. Mater. 57 (2015) 2–8.
[33] H. Etemadi, R. Yegani, M. Seyfollahi, The effect of amino functionalized and polyethylene glycol grafted nanodiamond on anti-biofouling properties of cellulose acetate membrane in membrane bioreactor systems, Sep. Purif. Technol. 177 (2017) 350–362.
[34] P. Karami, A. Shojaei, Morphological and mechanical properties of polyamide 6/ nanodiamond composites prepared by melt mixing: effect of surface functionality of nanodiamond, Polym. Int. 66 (2017) 557–565.
[35] P. Karami, B. Khorshidi, J.B.P. Soares, M. Sadrzadeh, Fabrication of highly permeable and thermally-stable reverse osmosis thin film composite polyamide membranes, ACS Appl. Mater. Interfaces 12 (2020) 2916–2925.
[36] V.N. Mochalin, I. Neitzel, B.J.M. Etzold, A. Peterson, G. Palmese, Y. Gogotsi, Covalent incorporation of aminated nanodiamond into an epoxy polymer network, ACS Nano 5 (2011) 7494–7502.
[37] B. Suart, Infrared Spectroscopy: Fundamentals and Applications, J. Wiley, Chichester, West Sussex, England; Hoboken, NJ, 2004.
[38] E. Ferrero, S. Navea, C. Repolles, J. Bacardit, J. Malfeito, R.D.-A. Agua-Spain, Analytical methods for the characterization of reverse osmosis membrane fouling, in: IDA World Congr. Proceedings, Pap. IDAWC/PER11-240, 2011.
[39] Z.F. Cui, Y. Jiang, R.W. Field, Fundamentals of pressure-driven membrane separation processes, in: Membr. Technol, Elsevier, 2010, pp. 1–18.
[40] B. Khorshidi, T. Thundat, B.A. Fleck, M. Sadrzadeh, Thin film composite polyamide membranes: parametric study on the influence of synthesis conditions, RSC Adv. 5 (2015) 54985–54997.
[41] Y. Qin, S. Yu, Q. Zhao, G. Kang, H. Yu, Y. Jin, Y. Cao, New insights into tailoring polyamide structure for fabricating highly permeable reverse osmosis membranes, Desalination 499 (2021), 114840.
[42] S. Karan, Z. Jiang, A.G. Livingston, Sub–10 nm polyamide nanofilms with ultrafast solvent transport for molecular separation 348 (2015) 1347–1351.
[43] A. Zhou, C. Shi, X. He, Y. Fu, A.W. Anjum, J. Zhang, W. Li, Polyarylester nanofiltration membrane prepared from monomers of vanillic alcohol and trimesoyl chloride, Sep. Purif. Technol. 193 (2018) 58–68.
[44] M. Rastgar, A. Karkooti, A. Sohrabi, P. Karami, N. Nazemifard, M. Sadrzadeh, Osmotic dewatering accelerates inherent sluggish kinetics of electro-Fenton process: toward sustainable removal of organic contaminants, Chem. Eng. J. 394 (2020), 125043.
[45] D. Chen, Q. Chen, T. Liu, J. Kang, R. Xu, Y. Cao, M. Xiang, Influence of l-arginine on performances of polyamide thin-film composite reverse osmosis membranes, RSC Adv. 9 (2019) 20149–20160.
[46] M.F. Ismail, B. Khorshidi, M. Sadrzadeh, New insights into the impact of nanoscale surface heterogeneity on the wettability of polymeric membranes 590 (2019), 117270.
[47] S. Xu, F. Li, B. Su, M.Z. Hu, X. Gao, C. Gao, Novel graphene quantum dots (GQDs)-incorporated thin film composite (TFC) membranes for forward osmosis (FO) desalination, Desalination 451 (2019) 219–230.
[48] J.A. Idarraga-Mora, M.A. Lemelin, S.T. Weinman, S.M. Husson, Effect of short-term contact with C1–C4 monohydric alcohols on the water permeance of MPD-TMC thin-film composite reverse osmosis membranes 9 (2019) 92.
[49] L. Zheng, W.E. Price, L.D. Nghiem, Effects of fouling on separation performance by forward osmosis: the role of specific organic foulants, Environ. Sci. Pollut. Res. 26 (2019) 33758–33769.
[50] X. Hao, S. Gao, J. Tian, S. Wang, H. Zhang, Y. Sun, W. Shi, F. Cui, New insights into the organic fouling mechanism of an in situ ca 2+ modified thin film composite forward osmosis membrane, RSC Adv. 9 (2019) 38227–38234.
[51] H. Mahdavi, A. Rahimi, Zwitterion functionalized graphene oxide/polyamide thin film nanocomposite membrane: towards improved anti-fouling performance for reverse osmosis, Desalination 433 (2018) 94–107.
[52] Z. Yang, Y. Wu, J. Wang, B. Cao, C.Y. Tang, In situ reduction of silver by polydopamine: a novel antimicrobial modification of a thin-film composite polyamide membrane, Environ. Sci. Technol. 50 (2016) 9543–9550.
[53] M. Raeiszadeh, F. Taghipour, Inactivation of microorganisms by newly emerged microplasma UV lamps, Chem. Eng. J. 413 (2021), 127490.
[54] J. Wehling, R. Dringen, R.N. Zare, M. Maas, K. Rezwan, Bactericidal activity of partially oxidized nanodiamonds, ACS Nano 8 (2014) 6475–6483.
[55] S. Szunerits, A. Barras, R. Boukherroub, Antibacterial applications of nanodiamonds, Int. J. Environ. Res. Public Health 13 (2016) 413.
[56] H. Etemadi, R. Yegani, V. Babaeipour, Study on the reinforcing effect of nanodiamond particles on the mechanical, thermal and antibacterial properties of cellulose acetate membranes, Diam. Relat. Mater. 69 (2016) 166–176.
[57] A. Chatterjee, E. Perevedentseva, M. Jani, C.-Y. Cheng, Y.-S. Ye, P.-H. Chung, C.-L. Cheng, Antibacterial effect of ultrafine nanodiamond against gram-negative bacteria Escherichia coli, J. Biomed. Opt. 20 (2014) 51014.
[58] S.F. Seyedpour, M. Dadashi Firouzjaei, A. Rahimpour, E. Zolghadr, A. Arabi Shamsabadi, P. Das, F. Akbari Afkhami, M. Sadrzadeh, A. Tiraferri, M.A. Elliott, Toward sustainable tackling of biofouling implications and improved performance of TFC FO membranes modified by ag-MOFs nanorods, ACS Appl.Mater. Interfaces 12 (2020) 38285–38298.
[59] M. Pejman, M. Dadashi Firouzjaei, S. Aghapour Aktij, P. Das, E. Zolghadr, H. Jafarian, A. Arabi Shamsabadi, M. Elliott, M. Sadrzadeh, M. Sangermano, ACS Appl.Mater. Interfaces 12 (2020) 36287–36300.
[60] M. Pejman, M.D. Firouzjaei, S.A. Aktij, E. Zolghadr, P. Das, M. Elliott, M. Sadrzadeh, M. Sangermano, A. Rahimpour, A. Tiraferri, Effective strategy for UV-mediated grafting of biocidal ag-MOFs on polymeric membranes aimed at enhanced water ultrafiltration, Chem. Eng. J. 130704 (2021).
[61] A. Mollahosseini, A. Rahimpour, M. Jahamshahi, M. Peyravi, M. Khavarpour, The effect of silver nanoparticle size on performance and antibacteriality of polysulfone ultrafiltration membrane, Desalination 306 (2012) 41–50.